Investigation of the Effects of Low-Pressure Carburizing Process Parameters on Microstructural Evolution by Means of In Situ Synchrotron X-Ray Diffraction

Ogün Baris Tapar,* Matthias Steinbacher, Jens Gibmeier, and Jérémy Epp

In situ X-ray diffraction experiments during low-pressure carburizing processes are performed at the German Electron Synchrotron Facility, Beamline P07, in Hamburg, Germany, with a specially developed process chamber. Microstructural evolution is precisely analyzed based on diffraction data, and several process parameters are varied. The investigations focus on boost and diffusion steps in which carbon donor gas interacts with the hot steel surface and carbon atoms diffuse through the sample. An increased process temperature leads to higher carbon absorption during the boost step, especially at the early stages of the process. Regardless of process parameters, austenite saturation is reached in a few seconds. Therefore, longer boost step duration and/or a higher acetylene amount does not directly increase the carbon profile; instead, this would only increase the amount of carbides formed on the surface, which would contribute to the carbon profile by dissolution in the following steps. Therefore, shorter and a high number of boost steps are recommended for high efficiency. The cementite formation rate shows a similar trend with austenite saturation. It is very fast at the beginning and then stays almost constant. Therefore, introducing acetylene to the furnace after that point has no positive effect on the carburization.

O. B. Tapar, Dr. M. Steinbacher, Dr. J. Epp
Department of Materials Science
Leibniz Institute for Materials Engineering
Badgasteiner Str. 3, Bremen 28359, Germany
E-mail: tapar@iwt-bremen.de

Dr. M. Steinbacher, Dr. J. Epp
MAPEX Centre for Materials and Processes
University of Bremen
Badgasteiner Str. 3, Bremen 28359, Germany

Dr. J. Gibmeier
Karlsruhe Institute of Technology
Institute for Applied Materials (IAM)
Kaiserstrasse 12, Karlsruhe 76131, Germany

The ORCID identification number(s) for the author(s) of this article can be found under https://doi.org/10.1002/adem.202100124.

1. Introduction

Case hardening based on gas carburizing and subsequent quenching of steel is an established method to produce high-performance components in the automobile and aircraft industry because it provides a hard, wear-resistant surface along with high core ductility.[1] Low pressure carburizing (LPC) has been gaining significance, especially in these industries as a surface-hardening procedure. Compared with conventional gas carburizing, LPC offers higher quality parts without oxidation, shorter process time because it has a wide temperature range from 880 to 1050 °C,[2] and highly reduced resource consumption, which is primary due to the very low amount of process gas required.[3,4]

LPC involves supplying of carbon to the surface of the material at generally 880–1050 °C temperature and under 1–30 mbar process pressure. During the process, the part is heated to the process temperature and carbon donor gas is introduced into the furnace under vacuum conditions; afterward, carbon atoms are released as a result of the catalytic effect of the surface of the steel with the carburizing atmosphere, and being absorbed on the steel surface.[5] This step is generally called the "boost step" and takes place under nonequilibrium condition because there is an unlimited carbon supply in this step. Subsequently, the furnace is evacuated from the remaining carbon donor gases to let the carbon diffuse toward the core of the steel. Thus, the carbon content close to the surface decreases with solid-state diffusion, which results, in the end, in a carbon profile with increasing depth. This step is generally called the "diffusion step." Cyclic boost and diffusion steps can be applied to achieve the desired carbon profile. After the desired carbon profile is reached, the components are generally quenched with a high-pressure inert gas such as helium or nitrogen or in oil, to get a martensitic microstructure. In today's industry, acetylene (C_2H_2) and propane (C_3H_8) are the most advantageous and highly used gases for LPC.[6] However, LPC using acetylene is particularly economical and environmentally friendly,[7,8] as well as being more effective because acetylene directly participates in the carburizing reactions rather than decomposing to other carburizing gases by pyrolysis.[9]

During the LPC process, the solubility limit of austenite can easily be exceeded and a cementite layer can be formed at the surface.[5,10–12] In a previous study, this could be confirmed by first evaluation of synchrotron diffraction data and it could be demonstrated that for a specific acetylene flow rate and sample geometry, the saturation limit of austenite in boost steps was reached in less than 10 s and cementite immediately formed at the surface of the material.[13] Due to the fast carbon accumulation and formation of cementite, the degree of carbon transfer from the atmosphere to the sample surface reduced, so the carbon-enrichment process was limited by the material. In the following diffusion step, the formed carbides dissolved within several minutes and contributed to the carbon content of the case. It is also known that alloying elements such as Cr promote carbide formation and reduce the solubility limit of austenite[14–16]; therefore, austenite saturation can be reached in even less than 10 s for high-alloyed steels. This means that the formation of cementite and other carbides is almost inevitable during any kind of LPC. As this hard and brittle layer is detrimental for the further processing and for service properties, understanding the effect of particular process parameters on the microstructural evolution, especially on carbide formation/dissolution in the boost step, is of high importance.

The aim of this study, therefore, is to describe the effect of critical process parameters on the microstructural evolution in boost and diffusion steps of LPC. For this, in situ synchrotron X-ray diffraction experiments were performed during complete LPC process at the Deutsches Elektronen-Synchrotron (DESY), Beamline P07, in Hamburg, Germany. Acetylene was used as the carbon donor gas. The microstructural changes were evaluated with spatial resolution of 20 μm height and time resolution of 0.2–0.5 s frame^{-1}. In addition, metallographic examinations of the final states after quenching were conducted to assess the results of the in situ analysis.

2. Experimental Section

2.1. Materials and Experimental Setup

An experimental LPC chamber and a control system were developed to perform in-situ X-ray diffraction experiments during the entire LPC process to analyze the microstructural evolution. **Figure 1** shows a sketch and a picture of the experimental setup.
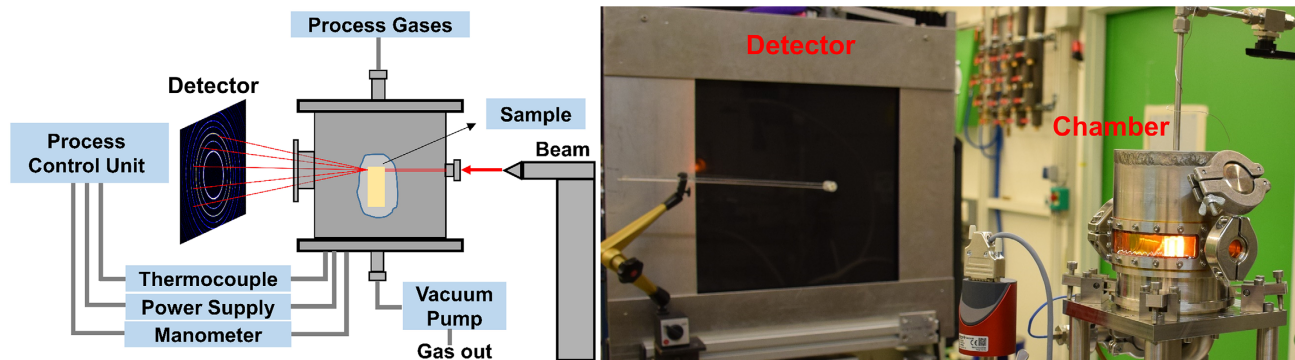
Table 1. Chemical composition in ma% of case hardening steel AISI 5120 (EN 20MnCr5).

C	Si	Mn	P	S	Cr	Mo	Ni	Al	Cu
0.2	0.25	1.26	0.017	0.031	1.26	0.030	0.039	0.030	0.024

Experiments with different process parameters were conducted and diffraction images were continuously recorded at different positions from the carburized surface.

Standard AISI 5120 (EN 20MnCr5) case hardening steel with 14 mm width, 14 mm height, and 5 mm depth was used as a sample. Samples were cut from annealed-state steel rods in the same direction to minimize the texture effect. The hardness was homogenously distributed over the samples with an average of 196.5 HV1 and the initial microstructure consisted of a homogeneously distributed ferrite–pearlite mixture. The chemical composition of the steel is given in **Table 1**.

All surfaces, except the top surface (5×14 mm^2 area) that was aimed to be carburized, were coated with ZrN using the PVD method to suppress the diffusion of carbon from the side surfaces (see **Figure 2**). The effectiveness of the coating was proved by comparing the carbon diffusion depth profiles of coated and uncoated samples after the carburization process in an industrial furnace with the same process parameters. After the comparison, only slight increase of carbon in a thin layer of these surfaces was observed. This increase is considered neglectable, since it contributed only to 0.1% of total X-ray signal stemming from the entire 5 mm thickness. Details about this comparison can be found in a previous study.[13]

The diffraction experiments were performed on Beamline P07-EH3 of the PETRA III Synchrotron at DESY/Hamburg with a high-energy monochromatic X-ray beam (103.4 keV), which permits working in transmission through the whole thickness of the steel sample. The primary beam height was adjusted to 20 μm in the direction of the carbon gradient using suitable slits and the beam width was chosen as 1000 μm to obtain high signal intensity and a good grain statistic. The definition of a beam height of 20 μm is a compromise between the required spatial resolution and the signal intensity of the diffracted beam. Full diffraction rings were recorded with acquisition times between 0.2 and 0.5 s frame^{-1} using a 2D detector (Perkin-Elmer with 2048×2048 px and a pixel size of 200 μm) placed 1.32 m behind

Figure 1. Sketch of the experimental setup for the in situ XRD measurement during LPC and a picture of the chamber in the hutch.
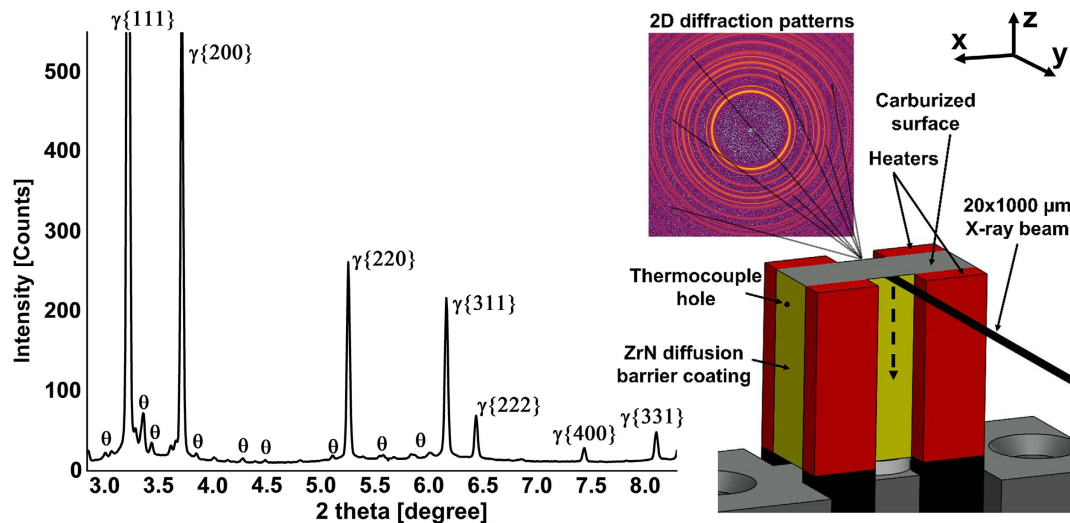
Figure 2. Integrated diffraction patterns (intensity vs 2θ), alignment of the sample and 2D-detector image showing the Debye–Scherrer rings of contributing {hkl} planes of the γ-phase (austenite) and the θ (cementite). Data belong to a sample during boost step measured at the tip of the sample. The sample was scanned in the direction of the dashed arrow by translating the sample to the z-axis.

the sample. Although there were some exceptions, the acquisition time of 0.2 s $frame^{-1}$ was adjusted for the steps with rapid microstructure evolution, such as the quenching and boost steps, and the acquisition time of 0.5 s $frame^{-1}$ was used during the diffusion step. The measured 2θ range was 0°–12.5°. The beam position was always kept fixed directly at the surface with an acquisition time of 0.2 s $frame^{-1}$ during the boost steps by keeping the sample stable. Thus, the measurement was made from the surface to max. 20 μm depth (beam height). As it was desired to focus at the surface as much as possible, the probed height was generally less than 20 μm. During the diffusion steps, the beam was either kept at a fixed position directly at the surface or the sample was continuously scanned through the synchrotron beam from the top surface to a depth of ≈500 μm by translating the sample stepwise in vertical direction z with 0.5 s $frame^{-1}$ acquisition time plus ≈4 s for z-translation for each position (see Figure 2).

Figure 2 shows a representative example of integrated diffraction patterns with {hkl} planes in the 2θ range covered by the 2D detector, and the 2D detector image with the 2D diffraction rings of contributing phases and alignment of the sample with heating elements.

Process gases were adjusted with two mass-flow controllers, which were controlled by a Protherm 510 process control unit (PCU) from United Process Controls GmbH/Germany. The pressure was measured using a capacitance manometer and regulated by a remote-controlled electromagnetic valve.

The sample was heated up using SiN ceramic heating elements connected to an external power supply. The voltage of the power supply was also adjusted by the PCU. The temperature was measured using a K-type mantle thermocouple inserted into a hole at the side of the sample and data were recorded using a Eurotherm temperature controller from Schneider Electric Systems Germany GmbH/Germany. Using a thermocouple hole instead of welding the thermocouple enabled the sample to be replaced without replacing the thermocouple and also kept the thermocouple stable during all the process steps. When the

sample reached the process temperature, the process was started after 1–2 min to ensure temperature homogeneity.

The 2D diffraction patterns that were recorded by the 2D detector were integrated using the fast PyFAI software.[17] For a detailed analysis of the evolution of the lattice parameter and phase fractions, the integrated diffraction patterns were analyzed using the convolution-based Rietveld refinement implemented in TOPAS 6.0 Academics (Coelho Software, Australia).[18] The fundamental parameter approach was used for the synthesis of generated peaks, based on the pseudo-Voigt function. TOPAS refinement was set regarding the generation of emission profiles and by convoluting instrumental contribution functions. The instrumental contributions to the diffraction peak profiles were determined using measurements of a 5 mm thick (same as sample thickness) standard LaB_6 NIST SRM660C powder sample. The determined fitting parameters were then fixed and used as instrumental function for the data analysis. For the proper refinements, convolutions of microstructure contributions, represented by crystallite size and microstrain contributions, are refined. Each phase was represented with relevant structure functions that covered lattice parameters, phase density, scale factors, and the temperature factor. After the best fit was achieved, the required parameters such as lattice parameters could be gathered for each phase.[19] During boost and diffusion steps, only austenite, which has a space group of Fm-3m [225], and cementite $(Fe,Cr)_3C$, which has a space group of Pnma [62], were taken into account.

2.2. LPC

2.2.1. Effect of Process Temperature

The industry temperature range for LPC is generally 880–1050 °C but most of the processes are conducted between 910 and 980 °C for conventional case hardening grades. A higher processing temperature shortens the processing time significantly and therefore reduces the cost. In particular,

Table 2. Process parameters for the experiments with varying temperature.

	Boost 1	Diff. 1	Boost 2	Diff. 2
Duration [min]	1	20	1	20
Pressure [mbar]	4	10^{-1}	4	10^{-1}

Table 3. Process parameters for the experiments with varying acetylene amount.

		Boost 1	Diff. 1	Boost 2	Diff. 2
Experiment 1	Duration [min]	5	20	5	20
	Pressure [mbar]	10	10^{-1}	10	10^{-1}
	Flow rate [mL min^{-1}]	10	0	10	0
Experiment 2	Duration [min]	10	20	10	20
	Pressure [mbar]	2	10^{-1}	2	10^{-1}
	Flow rate [mL min^{-1}]	80	0	80	0

temperatures higher than 980 °C are generally not desired due to detrimental grain growth,[1,20] and because of the risk of soot formation.[21]

To investigate the effect of temperature on the microstructural evolution, two LPC experiments were conducted at 920 and 960 °C, respectively, with the same parameters given in **Table 2**.

Before the process, the chamber was evacuated to 10^{-1} mbar and the samples were heated up to the process temperature with a heating rate of 2 K s^{-1} to achieve a full austenitic state. After that, acetylene was continuously steamed into the furnace. The bottle outlet pressure of acetylene was adjusted to slightly over atmospheric pressure of 1.2 bar and a flow rate of 10 mL min^{-1} ($\approx$8 m^3 m^{-2} h^{-1}) to initiate the boost step and the process pressure went up to 4 mbar. In the following diffusion step, the remaining acetylene was extracted from the furnace; therefore, the pressure reduced back to 10^{-1} mbar. This boost/diffusion cycle was repeated two times in total. Details of the durations are given in Table 2. After the final diffusion step, the samples were quenched with 5 bar helium gas with gas flow directed at the top surface of the sample. A representative process scheme is shown in **Figure 3**.

2.2.2. Effect of Acetylene Amount

The degree of dissociation of the carburizing gas depends on the temperature and flow rate, so correct selection of the flow rate of the carbon donor gas is very significant for the process efficiency.[22,23] The optimum amount of carburizing gas varies a lot depending on the process temperature, batch size, and complexity of sample geometry; therefore, modern LPC processes are conducted using an excess amount of carbon donor gas. This creates a very high carbon potential and fast saturation of the austenite. Therefore, understanding the microstructural evolution during the boost steps is crucial for gaining an appropriate process comprehension.

To investigate the effect of the acetylene amount on the microstructural evolution, two different LPC experiments with two boost steps were planned and conducted at 940 °C. The amount of acetylene can be varied by increasing the duration of the boost step, by increasing the acetylene flow rate, or by increasing both
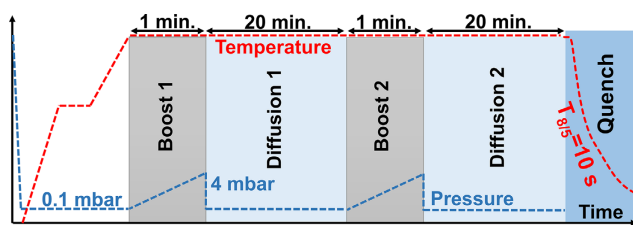
of them at the same time. Therefore, in experiments given in **Table 3**, not only single parameter was varied.

For both experiments, the chamber was first evacuated down to 10^{-1} mbar and subsequently the sample was heated to 940 °C with a heating rate of 2 K s^{-1}. Then, acetylene was introduced into the furnace. The acetylene bottle outlet pressure was 1.2 bar. Details of flow rates and durations are provided in Table 3. During the boost steps of experiment 1, the vacuum valve was closed. As a consequence, the average pressure in the chamber during the boost step was 10 mbar; for experiment 2, instead, the vacuum valve stayed open, so the sample was showered with acetylene at constant 2 mbar pressure. The experimental chamber was designed in a way that the gas inlet pipe was placed directly above the carburized and investigated surface, and the vacuum outlet pipe was placed right at the bottom of the sample. Therefore, the sample was placed in the direction of the gas flow. With this strategy, the optimum pressure range for the processes was not exceeded and the sample was exposed to a very high amount of acetylene. The acetylene amount is linked with the pressure; thus, adjusting different acetylene amounts under the same pressure is not possible in our system due to technical limitations. However, according to a study performed in a thermogravimetric measurement device to determine the mass gain during carburizing, no significant differences were observed between absolute acetylene pressures of 3–15 mbar.[24] Therefore, the values were tried to be adjusted as close as this pressure interval and the effect of pressure was neglected in this study. However, pressure information was still included in the table to be more specific about experiments.

2.2.3. Effect of Boost-Diffusion Cycles

When a high case hardening depth (CHD) is desired, the number of boost-diffusion cycles is generally increased and the carbon gradient becomes flatter. The addition of supplementary boost steps makes the prediction of the microstructural evolution difficult. Therefore, understanding of the effect of a higher number of boost steps is crucial to provide appropriate predictions.

To investigate the effect of the number of cycles, an experiment with four boost steps was conducted at 940 °C, and results were compared with those of the standard experiment. Experiments were started with the same procedure and parameters as described in the previous sections. The diffusion pressure was 10^{-1} mbar, and the flow rate and bottle outlet pressure

Figure 3. Process scheme of two boost-diffusion-cycle LPC experiment.

Table 4. Duration and pressure of boost and diffusion steps of two experiments.

		B1	D1	B2	D2	B3	D3	B4	D4
CHD[a)]	Duration [min]	1	20	1	20	1	30	1	45
	Pressure [mbar]	4	10^{-1}	4	10^{-1}	4	10^{-1}	4	10^{-1}
Standard	Duration [min]	1	20	2	20	1	25	–	–
	Pressure [mbar]	4	10^{-1}	8	10^{-1}	4	10^{-1}	–	–

[a)]The first two boost-diffusion cycles of this sample are the same as those in Table 2; therefore, this sample can also be compared with samples in Section 2.2.1. as an example of 940 °C. To eliminate repetition, the results of this sample were not also given in that section.

of acetylene were 10 mL min^{-1} and 1.2 bar, respectively. Process pressures and durations of four boost-diffusion cycles are given in **Table 4**.

3. Results

3.1. Effect of Process Temperature

Two samples were carburized at different temperatures. During the process, changing of the peak position, full width at half maximum (FWHM), and integrated intensity was observed. **Figure 4** shows the change of peak positions, FWHM, and integrated intensities of γ {111} and γ {200} austenite peaks during boost steps.

During the boost step, the measurement was performed from surface to max. 20 μm beam height. The time scale started at time zero, where the acetylene valve was opened. After about 5–7.5 s for all the boost steps, the first shift of the initial positions of given austenite peaks to lower 2θ angles can be clearly observed.

Intensity differences during peak shifting can also be noted in the figure for both samples. Any atmospheric changes such as change of the condition of the vacuum valve or cold acetylene gas introduction to the furnace cause the temperature to drop sharply by ≈10–15 °C, which causes the sample to shrink and relatedly the gauge volume probed by the stationary synchrotron beam to shift toward the top of the sample due to this sample contraction. Therefore, at the beginning of every boost step, when the vacuum valve position is changed from open to closed, the intensity suddenly reduces and continues to increase while the temperature increases. In addition, the intensity again reduces when acetylene first contacts with the sample, which is after ≈5–10 s because the nominal gauge volume is only partially filled with material. To compensate for this kind of temperature-related problems, entry scans were applied to find the surface precisely. After that, the position of the sample was not changed. Furthermore, adjustment of the temperature was also made when necessary to retain the process temperature as fast as possible. Although this kind of change could not be fully eliminated, this would not affect the final results of carbon content critically since the final intensity values are very close to each other. In addition, the carbon content is calculated using the lattice parameter, which is directly related to the peak position,

not the peak intensity. This is confirmed by the consistency of the final results of the lattice parameter and carbon content. The reason that this effect is not consistently observed and therefore not precisely predicted is that there are also exothermic acetylene decomposition reactions taking place at the surface, which balance the temperature decrease due to cold acetylene contact and valve opening. Therefore, this effect was observed with variant extents in several samples, and it is very difficult to eliminate.

An increase of the FWHM related to peak broadening can also be observed during the boost steps at the same time peak shifting is first detected. Therefore, this effect is mainly attributed to the change of carbon inhomogeneity in the sample due to the dissolution of carbon in austenite, which is discussed in more detail in Section 4.

During the first boost step of both samples, peak shifting to the lower angle can be observed. For the sample carburized at 920 °C, peak shifting starts after ≈7.5 s; for the sample carburized at 960 °C, peak shifting starts after ≈5 s. The initial peak positions of both samples are 3.255° for γ {111} peaks and 3.7575° for γ {200} peaks. Peaks of the sample carburized at 960 °C shift to smaller angles than those of the sample carburized at 920 °C. During the second boost steps, peak shifting to a lower angle is also observed. However, contrary to the first boost step, the positions of the peak do not continuously shift to lower angles, but rather stay almost constant after ≈30 s until the end of the step.

The boost steps were followed by diffusion steps with 20 min duration (see Table 2). The change of peak positions, FWHM, and integrated intensities of γ {111} and γ {200} austenite peaks during the first diffusion step of 920 °C can be seen in **Figure 5** as a representative example. The first scans of the data are not shown in the figure because of the 0.5–1 min time required for transition of the measurement modus from stable mode to scanning mode.

During diffusion steps, the sample was scanned continuously several times from top to ≈0.5 mm depth. Integrated intensity values are very low when only a minor part of the sample is probed in early seconds of individual scanning; however, they increase to the interval of 55–65 units for the γ {111} peak and 22–30 units for the γ {200} peak when all of the 20 μm beam height is in the sample. Before each boost step, similar entry scans were performed and these intervals at which data points are maximum/constant were set as a measurement intensity interval for all the samples.

FWHM values are higher at the beginning of the scan due to the smaller peak heights and carbon inhomogeneity of the sample at the top surface where the scan begins. When scanning continues toward the depth, FWHM values decrease to values between 0.026 and 0.030 degrees for both the γ {111} and γ {200} austenite peaks. A slow shift of the austenite peaks back to higher angles can be systematically observed in both individual scans and the overall evolution during the whole diffusion step.

The diffraction patterns of other diffusion steps of this sample and other samples are not displayed in this form because they are very similar to these graphs but they were examined in detail by evaluation of lattice parameters in Section 4.

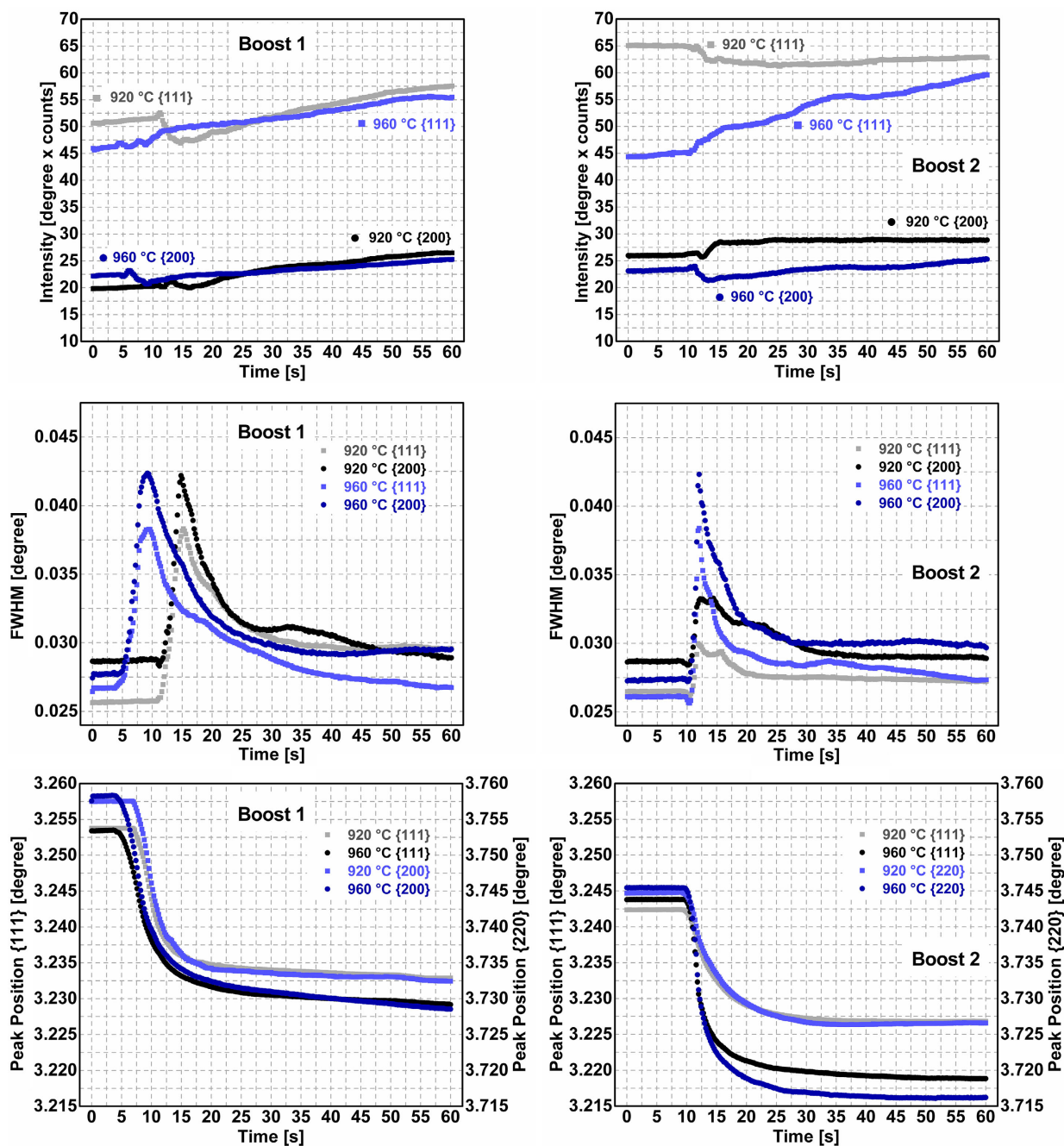Note also that the intensity and relatedly FWHM are not stable, although the whole 20 μm beam height was on the

**ADVANCED
SCIENCE NEWS**

www.advancedsciencenews.com

**ADVANCED
ENGINEERING
MATERIALS**

www.aem-journal.com

Figure 4. Change of peak positions, FWHM, and integrated intensities of γ {111} and γ {200} austenite peaks versus duration of the boost step for two different samples carburized at different temperatures. The average error margin for integrated intensity and FWHM is ±5% of data points and 4×10^{-4} degrees, respectively which are not shown in the figure due to the high number of data points. Error margins of peak positions are smaller than symbols.

sample. For example, the intensity of the γ {111} austenite peak fluctuates from 50 to 65 units and FWHM values fluctuate between 0.026 and 0.030 degrees. The two main reasons for this are the continuous change of carbon content in the probed area due to diffusion from the surface to depth and the earlier mentioned minor temperature changes. There was no visible effect of these fluctuations in lattice parameter examination and their degree is not high; therefore, they are not further considered.

3.2. Effect of Acetylene Amount

Two different experiments using a higher amount of acetylene were conducted (see Table 3). During the experiments, peak shift toward lower angles during the boost steps and toward higher 2θ angles during diffusion steps were observed and noted similar to the previous section for the other process variants. **Figure 6** shows the change of integrated intensities, FWHM, and peak
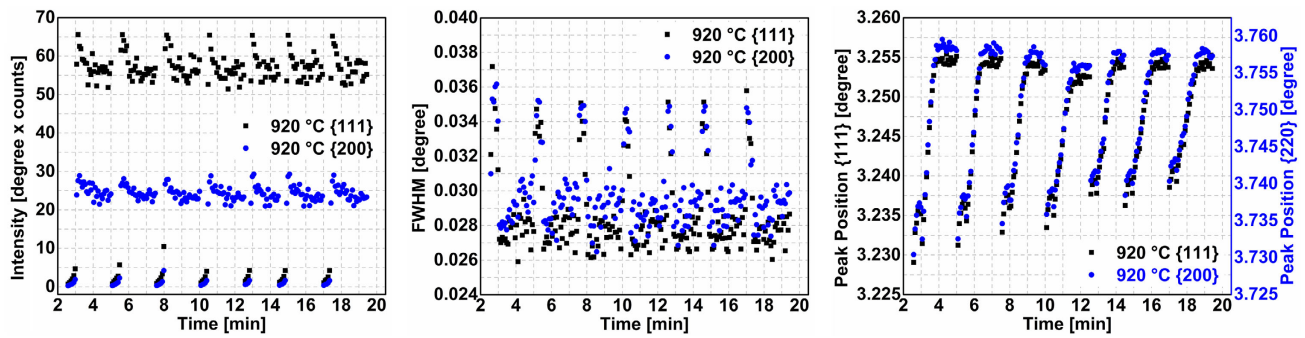
Figure 5. Change of peak positions, FWHM, and integrated intensities of γ {111} and γ {200} austenite peaks during scanning over the z-axis for the first diffusion step of the sample carburized at 920 °C. There are seven scan steps with about 2.5 min each from the top surface to ≈0.5 mm depth.

positions of γ {111} and γ {200} austenite peaks during boost steps.

The final peak positions in 2θ of the γ {111} and γ {200} peaks for experiment 1 and experiment 2 are comparable for both boost steps, with slightly greater shifting of that of experiment 2 to the lower angles. In addition, the peak shift during experiment 2, which has an 80 mL min^{-1} acetylene flow rate, occurs earlier and faster compared to experiment 1 having a 10 mL min^{-1} acetylene flow rate during the first boost step.

Similar to the samples described in the previous section, intensity changes can be observed for both samples. The intensity of peaks for the first boost step of experiment 2 starts at lower values and is corrected slowly after ≈150 s. Thus, the final intensities of experiment 1 and experiment 2 are very close. A similar behavior can also be observed for the second boost step in which intensities of both samples are lower at the beginning and they get to closer values until the end of the step. Moreover, similar FWHM increase at the point where peak shift occurs can also be observed for these samples. After this increase, the values again decrease slowly to ≈0.028–0.030 degrees.

3.3. Effect of Boost-Diffusion Cycles

An LPC experiment with four boost steps was conducted and the results were compared with the standard experiment using only three boost steps. The changes of integrated intensities, FWHM, and peak positions of the γ {111} and γ {200} austenite peaks during boost steps are shown in **Figure 7**.

During both experiments, a peak shift to lower angles was systematically observed. Although the duration of the second boost step reduced to half compared to the standard experiment, the final peak positions are comparable. Moreover, except for the first boost step, the final peak positions after each boost step were almost the same, but the initial positions varied depending on the diffusion step before each boost step.

Similar to the previous sections, the intensities start at lower values and increase until the end of every step except the third boost step of the CHD sample. During this step, about a 10% decrease in the intensity of both the γ {111} and γ {200} peaks can be observed. This decrease starts at the same point where peak shifting starts; thus, it is attributed to sample shrinkage caused by temperature decrease due to contact with cold

acetylene gas. The effect of this change is discussed in more detail in the next section. The change of FWHM for all boost steps is also similar to the ones observed in previous sections. FWHM values increase when shifting starts and decrease slowly until the end of each step.

4. Extended Analysis of In Situ Data and Discussion

4.1. Effect of Process Temperature

Peak shift toward lower and higher 2θ angles in the process is directly related to the change of the lattice parameter. After analyzing integrated diffraction patterns, the change of the austenite lattice parameter from the beginning of the first boost step to the end of the second diffusion step was acquired and is shown in **Figure 8** for both samples.

During the boost and diffusion steps, the temperature is mostly stable ($\pm15\,°C$ of the process temperature), and the sample is at fully austenitic temperatures and homogeneous in terms of composition, so it can be considered stress-free. Thus, at constant temperature, changes in the lattice parameter can only be attributed to changes in the chemistry, i.e., in the present case most likely to of the amount of carbon in solid solution in austenite. During the boost step, carbide formation was observed at the surface of the samples, which might generate stress on austenite. The effect of this stress on the peak shifting is assumed to be very low due to high temperatures; therefore, it is neglected in calculations and peak shifting is only attributed to the carbon content change.

The prediction of the carbon content can be done from the dilation of an austenite lattice parameter due to the occupation of octahedral sites of the austenitic lattice by the carbon atoms. For this, the model developed by Onink from neutron diffraction experiments taking into account the thermal effect was used.[25] According to the model, the lattice parameter of austenite is formulated as

$$a_\gamma = \left(0.363067 + 0.000783 x_C^f\right) \times \left[1 + \left(24.92 - 0.51 x_C^f\right) \times 10^{-6} \times (T - 1000)\right] \quad (1)$$

where x_C^f is the atomic percentage of carbon and T is the temperature in kelvin. This formula is modeled using pure iron but

ADVANCED
SCIENCE NEWS
www.advancedsciencenews.com

ADVANCED
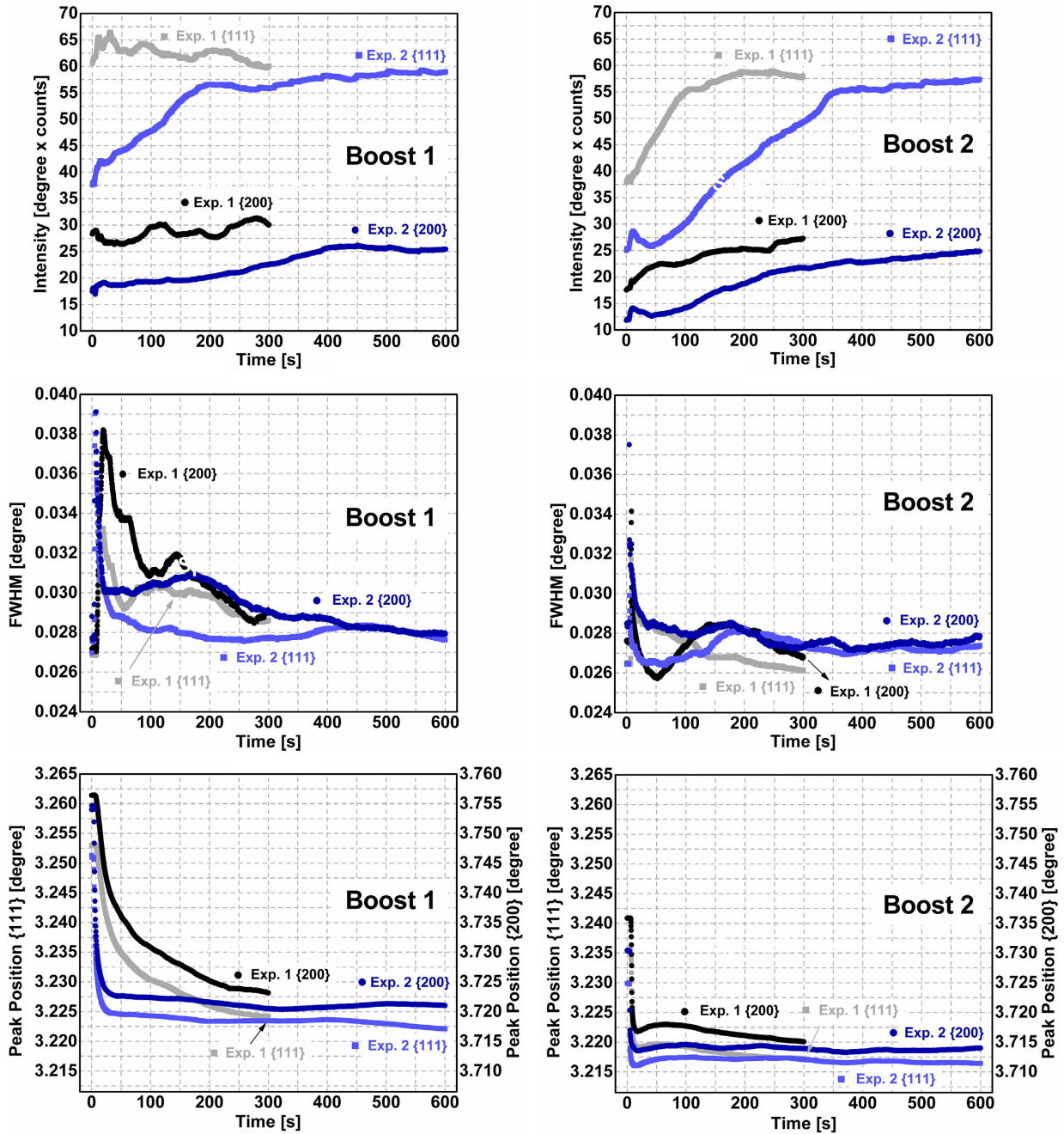**ENGINEERING**
MATERIALS
www.aem-journal.com

Figure 6. Change of integrated intensities, FWHM, and peak positions of γ {111} and γ {200} austenite peaks with time for the boost step of two different samples carburized with different acetylene amounts. The average error margin for the integrated intensity and FWHM is ±5% of data points and 3.7×10^{-4} degrees, respectively, which are not shown in the figure because of the high number of data point. The error margins of peak positions are smaller than the symbols.

studied steel has about 5 ma% alloying elements. Therefore, the base carbon content of 0.2 ma% was taken as a reference and the formula was tested according to this value. For most of the samples, the results were very accurate, so error margins are less than ±0.02 ma%. However, there were a few exceptions where the error margin was ≈±0.04ma%. Based on the determined deviation, all values were corrected and a ±0.04ma% error margin is

stated for carbon content calculations for the sake of safety. In addition, in a previous study by the authors, values determined by the given formula were compared with electron microprobe analyses results and the values were found to be very close.[13]

Figure 9 shows the change of the average carbon content dissolved in austenite during boost and diffusion steps for two different samples carburized at different temperatures after
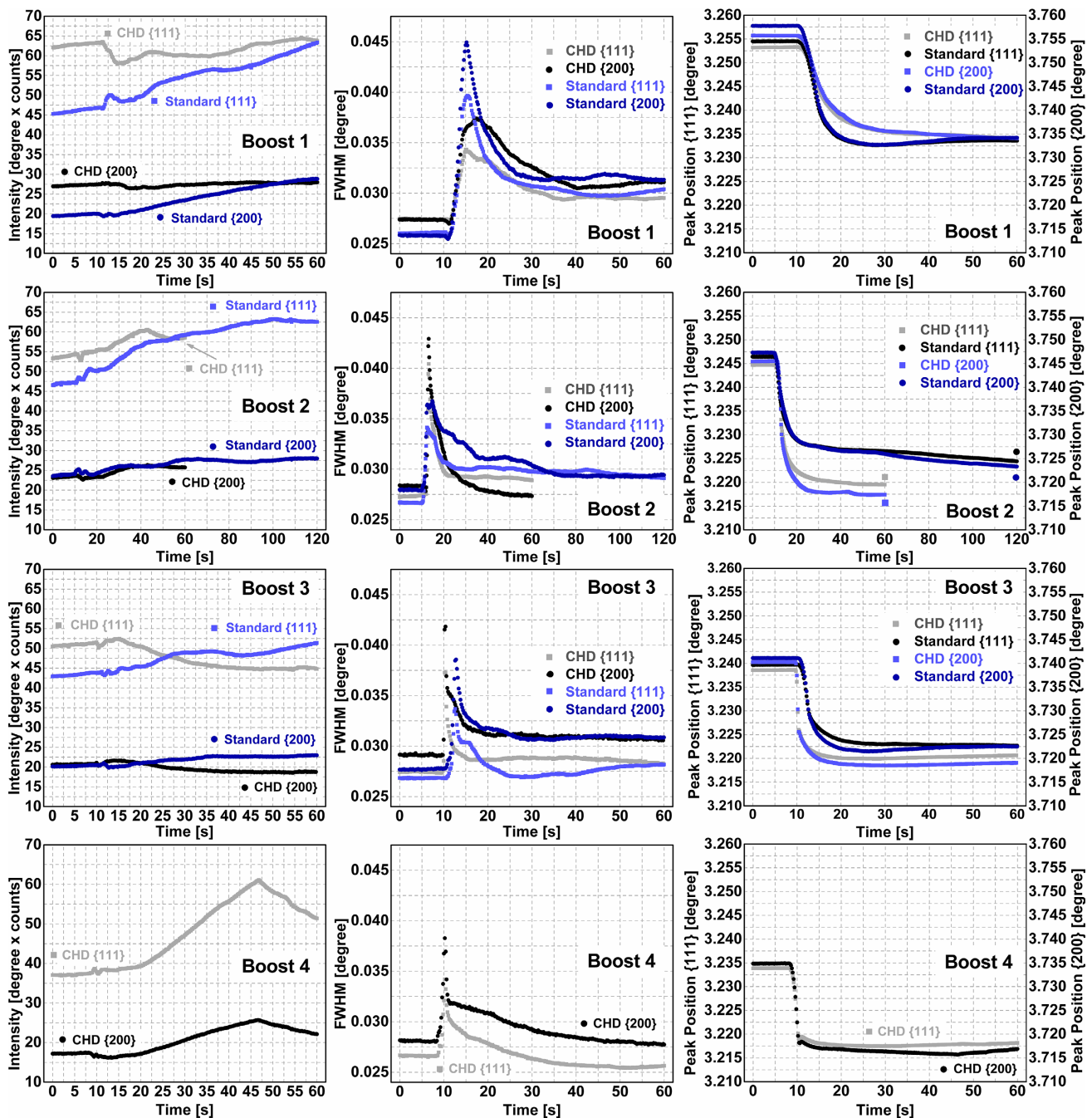
Figure 7. Change of integrated intensities, FWHM, and peak positions of the γ {111} and γ {200} austenite peaks with time for the boost step of two different samples carburized at 940 °C with different boost-diffusion cycles. The average error margin for the integrated intensity and FWHM is ±5% of data points and 3.3×10^{-4} degrees, respectively, which are not shown in the figure because of the high number of data point. The error margins of peak positions are smaller than the symbols.

conversion in ma%. During the boost steps, the beam position was kept constant on the surface, whereas during diffusion steps the samples were scanned from top to ≈500 μm surface distance. The investigated diffusion scans are shown in Figure 8 with black arrows.

The carbon content before the first boost step was calculated as 0.2 ma%, which is the base carbon content of the steel. During

the first boost step, the average carbon content of the low-temperature sample increased up to ≈0.95 ma%, while that of the higher temperature experiment went up to ≈1.05 ma%. This difference is attributed to the higher solubility limit of austenite at high temperature. According to the Thermocalc software, the maximum carbon solubility of steel used in this study is ≈1.33 ma% for 960 °C and ≈1.30 ma% for 940 °C. As the beam
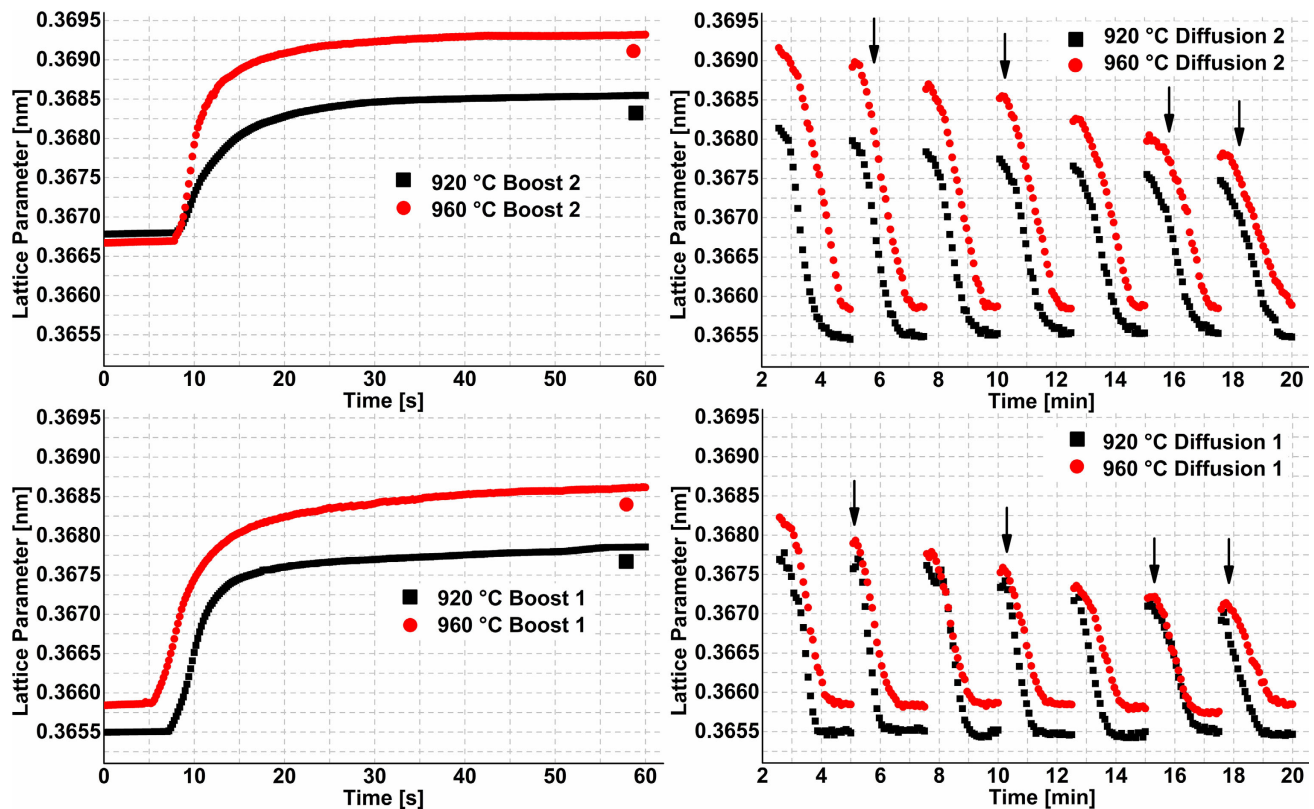
ADVANCED
SCIENCE NEWS
www.advancedsciencenews.com

ADVANCED
ENGINEERING
MATERIALS
www.aem-journal.com

Figure 8. Evolution of the lattice parameter of austenite for samples carburized at 920 and 960 °C. Black arrows in diffusion graphs show further investigated scans for the change of carbon content determination. The average error bar scale is $\mp 5 \times 10^{-5}$ and it is smaller than the symbols.

height is max. 20 μm, but the carbon accumulation in the austenite is first taking place with a strong gradient over the first microns from the surface, the average carbon content in the measured area is quite a bit lower than the maximum solubility limit of austenite at the specified temperatures. However, it gets closer to the maximum value in each boost step. Acetylene decomposes to carbon and hydrogen very rapidly when it contacts a hot steel surface,[26–28] which causes, about 10 s after the acetylene valve opening, carbon atoms to accumulate in austenite and the carbon content to increase sharply. Then, the rate of increase slows down continuously and tends to a steady-state condition.

One reason for this rate decrease for both samples can be the accumulation of carbon at the surface following the formation of a very fine continuous cementite (Fe_3C) layer in the first few microns of the surface. Carbide formation after the accumulation of surface was already observed in previous investigations,[13] and is confirmed for further process parameters. If the concentration of carbon at the surface during boost step exceeds the solubility limit of austenite, M_3C carbides, M being mostly Fe and Cr, can be generated on the surface.[29] This carbide layer decelerates the carbon uptake from the atmosphere to the sample and possibly hampers the diffusion of carbon in the near-surface region of the sample due to the lower diffusion speed of carbon in cementite.[30,31] Moreover, this carbide layer may passivate the surface (or some part of the surface) by blocking the reaction sides; therefore, the autocatalytic acetylene decomposition reaction is slowed down, so the available carbon amount decreases.[5,32–34]

In the following diffusion steps after the first boost steps, carbon contents of both samples were the same after 5 min, although a higher carbon content was reached during the boost steps for the higher temperature process. Moreover, the carbon content at the surface for the high-temperature process decreased faster in the following minutes of the diffusion step. This is due to the increased diffusion coefficient at high temperature as well as an increased driving force provoked by the steeper carbon gradient because of the higher surface carbon content. A similarly rapid decrease of surface carbon content can be observed for the second diffusion step analogously. In addition, the depth reached is much higher for the high-temperature process. At the end of the second diffusion steps, the carbon contents at 0.5 mm depth are ≈0.32 and 0.25 ma% for the high-temperature and low-temperature processes, respectively.

During the second boost step, similar to the first one, the carbon content increased very fast at the beginning for both samples. However, the starting value is not the nominal carbon content of the steel anymore, but a high value that remains after the previous diffusion step. After the first rapid increase within ≈10 to 20 s, the carbon content in solution in austenite at the surface remains mostly constant over the remaining boost duration, although acetylene was continuously introduced into the chamber at the same rate. The carbon content at the saturation level increased up to ≈1.12 ma% at 920 °C, while a value of up to ≈1.26 ma% is reached at 960 °C. The maximum solubility limits of the studied steel at 920 and 960 °C are ≈1.19 and ≈1.33 ma%,
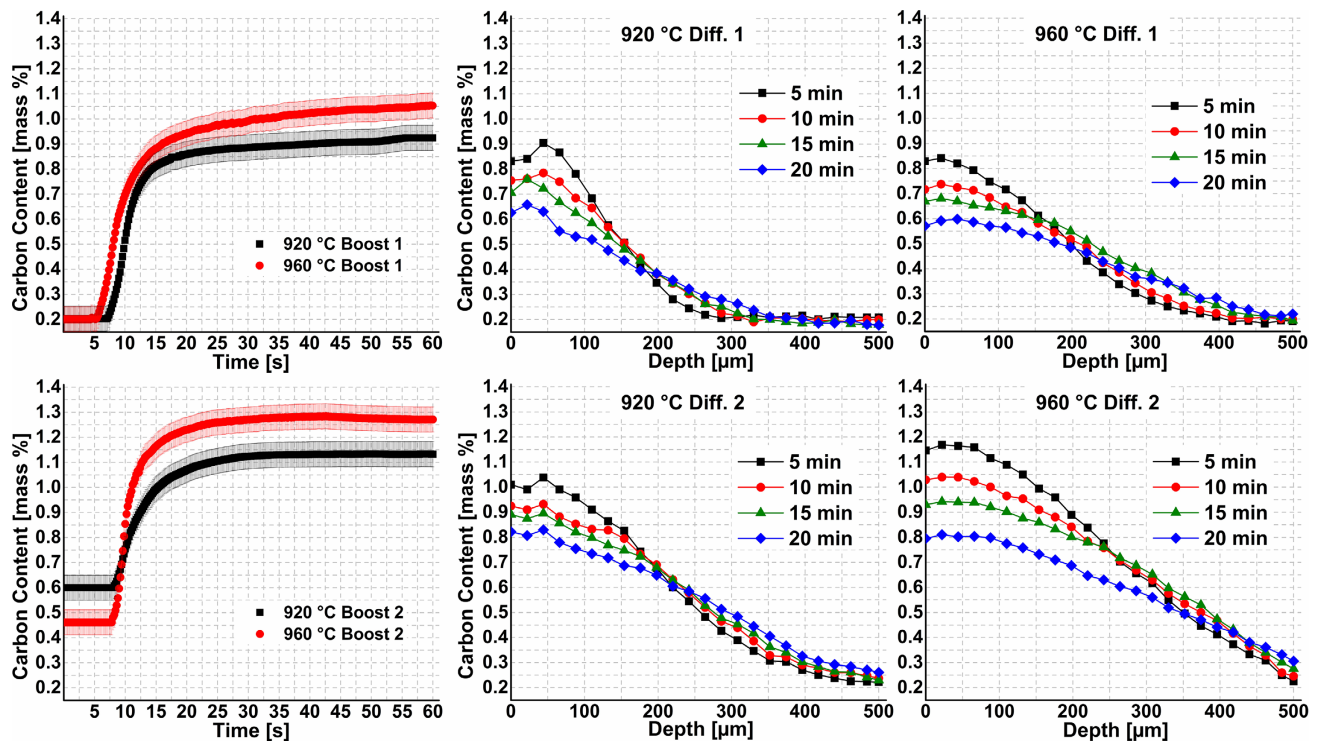
**ADVANCED
SCIENCE NEWS**
www.advancedsciencenews.com

**ADVANCED
ENGINEERING
MATERIALS**
www.aem-journal.com

Figure 9. Evolution of carbon content dissolved in austenite during the boost and diffusion steps of two samples carburized at 920 and 960 °C. $t = 0$ is the time that the acetylene valve was opened. Error margins for all graphs are ±0.04ma% as shown in boost steps. For diffusion steps, they are not given on the figure for the sake of clarity.

respectively. Measuring lower values than the indicated maximum limits is an indication that there is still a carbon gradient in the probed beam height of max. 20 µm area close to the very surface.

Based on the result, it can be said that the samples carburized at a higher temperature exhibit a steeper carbon content increase rate than the sample carburized at a lower temperature for both boost steps. Moreover, the final carbon content in the sample carburized at a high temperature is higher than that of the sample processed at a lower temperature, which is expected. The time required for initiation of carbon diffusion in austenite is lower for the first boost step of the high-temperature sample; however, it is similar in the second boost step, which is ≈8 s after the valve opening time; i.e., the observed effect is not consistent. Therefore, it can be said that there is no certain relation between the temperature and the point where the carbon content starts to increase.

In addition, it can be concluded for diffusion steps that the effect of temperature is more dominant at the early stages of the process and its effect gets lower during each additional step. This indicates that the main driver is the carbon gradient, which is flattening during the process. Carbon in the high-temperature process reached higher depths but the sample had a slightly lower surface carbon content, which is due to the increased diffusion coefficient. The difference of 40 °C temperature for the two processes conducted with the given parameters results in a variation of the surface carbon content between 0.05 and 0.08 ma% in the final carbon profiles.

The formation of carbides during the boost steps was confirmed as growing diffraction peaks belonging to cementite could be observed during the boost steps, as shown in **Figure 10**. It is very important to recall that the amount of carbon in solid solution in austenite is determined using a lattice parameter, which
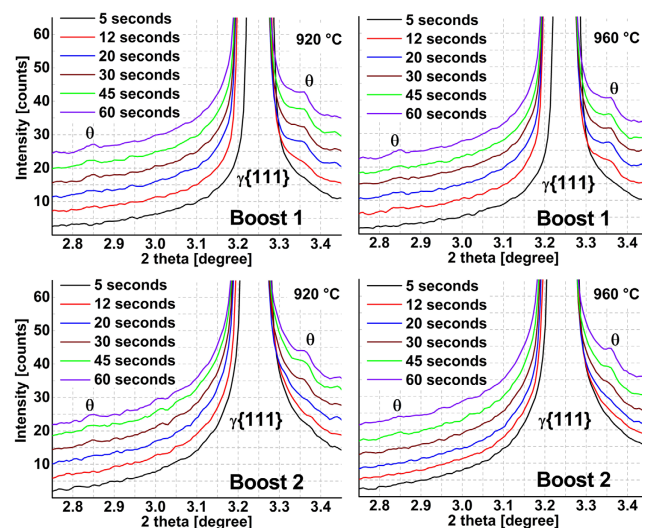

Figure 10. Cementite (Fe_3C/θ) formation near main γ {111} peak during the boost steps of samples carburized at 920 and 960 °C. The 5 s peak is the reference, and each peak after that was offset +3 from the previous one on the y-axis for easy examination.

**ADVANCED
SCIENCE NEWS**

www.advancedsciencenews.com

**ADVANCED
ENGINEERING
MATERIALS**

www.aem-journal.com

depends on the peak position, and does not represent the total amount of carbon. However, quantitative analyses of the carbides are done using the peak intensity. Between the steps, thermal expansion or shrinkage of the material causes the sample surface position to change and relatedly the relative intensities of the peaks to change. Although the variations were not significantly high and manually adjusted by increasing or decreasing the temperature, they might still affect the peak intensity of minority phases. Therefore, each figure should be interpreted individually for a quantitative deduction, especially when the peak intensities are very close.

There is no obvious difference between carbide peak intensities of both samples in the two boost steps. Thus, it is difficult to make a quantitative comparison. However, it can be seen from the partial figures that carbides start to form in the very early stages of the boost steps in different amounts, as soon as the surfaces of the samples are saturated with carbon (≈20–30 s after opening the acetylene flow), and grow until the end. Therefore, carbide formation is confirmed for both samples. Note also that from 5 s of the second boost step that carbides formed in previous steps are dissolved during the following diffusion.

To observe the carbide formation at the surface, one sample was gas quenched with helium directly after the boost step and the surface was scanned using synchrotron X-rays. **Figure 11** shows the metallographic examination of the sample and diffraction peaks of the surface.

According to X-ray diffraction and metallography results, 2–3 μm M_3C carbides, M being mostly Fe, Cr, and Mn, were detected on the surface of the sample directly after the boost step.

4.2. Effect of Acetylene Amount

Similar to previous investigations, peak shifts were observed during the boost and diffusion steps of both experiments. These peak shifts are again directly related to carbon absorption and
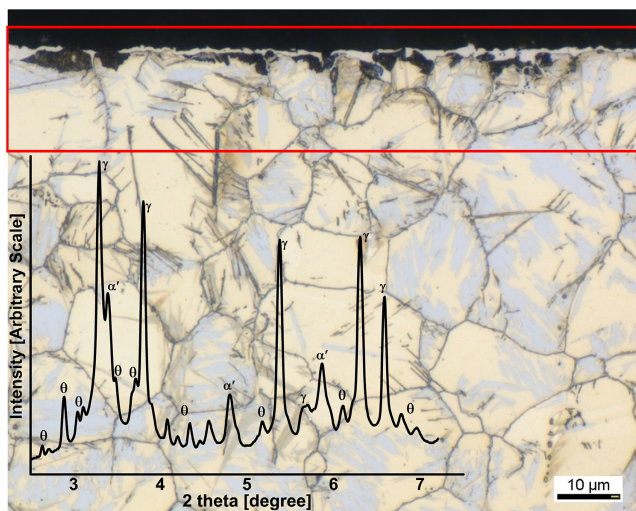

Figure 11. Metallographic examination and synchrotron X-ray diffraction results of the sample quenched directly after the boost step. The γ -phase in the diffraction pattern is austenite, the α′ phase is martensite, and θ is M_3C carbides. The standard metallography procedure was applied and the sample was etched with 3.5% nital. The probed area is indicated in red.

diffusion via the lattice parameter evolution. Integrated diffraction frames were analyzed and the lattice parameter changes were found using the same procedure as previously presented. **Figure 12** shows the change of lattice parameter of austenite during the boost and diffusion steps of two samples carburized with different acetylene amounts. During the 20 min of diffusion, a different measurement strategy was followed. Samples were scanned to 500 μm depths in the first and last 2.5 min to compare the initial and final carbon depth profiles. During the remaining 15 min between the scans, measurement was done at the very surface to observe the change in carbon content at the surface.

Slightly higher lattice parameter values for experiment 2 can be observed from the graph, especially for the second boost-diffusion cycle. Carbon contents dissolved in austenite were calculated using determined lattice parameters and Equation (1) for each of the boost and diffusion steps.

Figure 13 represents the calculated change of carbon content during boost and diffusion steps of the two different experiments.

In the first boost steps, at the very early stages, the carbon content in the measured volume increases rapidly. Carbon contents at the end of 60 s are ≈0.95 and 1.18 ma% for experiment 1 and experiment 2, respectively, which indicates that increasing the acetylene flow rate had a positive effect on carbon absorption from the atmosphere to the sample in the first minute. After the first minute of experiment 2, the carbon content stays almost constant at ≈1.18 ma%, but during experiment 1, it increases continuously. It seems that carbon supply to the surface of the sample during experiment 1 still continued very slowly after the first minute but for experiment 2 it stopped. Although the rate of carbon absorption decreases after the first minute, increasing the duration of the boost without changing the acetylene flow rate can still supply carbon to the surface at a very low rate. Therefore, it is interesting to note that the final carbon contents at the surface after the first boost step of these two experiments are very close despite the very different flow rates and durations. This is an indication that, after a certain point, which is most probably the coverage of the surface with carbides, which blocks the reaction sides, it is not possible to further increase the carbon before the formed carbides are dissolved.

In the second boost step, the amount of carbon content at the end of 60 s was ≈1.3 and 1.34 ma% for experiment 1 and experiment 2, respectively. Increasing the boost step duration to two times and flow rate to eight times higher values does not have a significant effect on the final carbon content. Especially, if the higher initial carbon content of experiment 2 was taken into account, the effect of a higher flow rate of acetylene and a longer duration of boost on the final carbon content seems not as pronounced as for the first boost step.

Note also that there is a peak point of carbon content in the 20th second of the seconds boost steps for both experiments, and then the carbon content decreases slightly by ≈0.02 ma%. The reason for this might be an accumulation of carbon at the beginning due to the high reactivity of the surface until cementite is built.

Similar to the temperature-variation case, carbide formation during the boost steps was also observed. **Figure 14** shows cementite peaks formed at the different stages of boost steps.
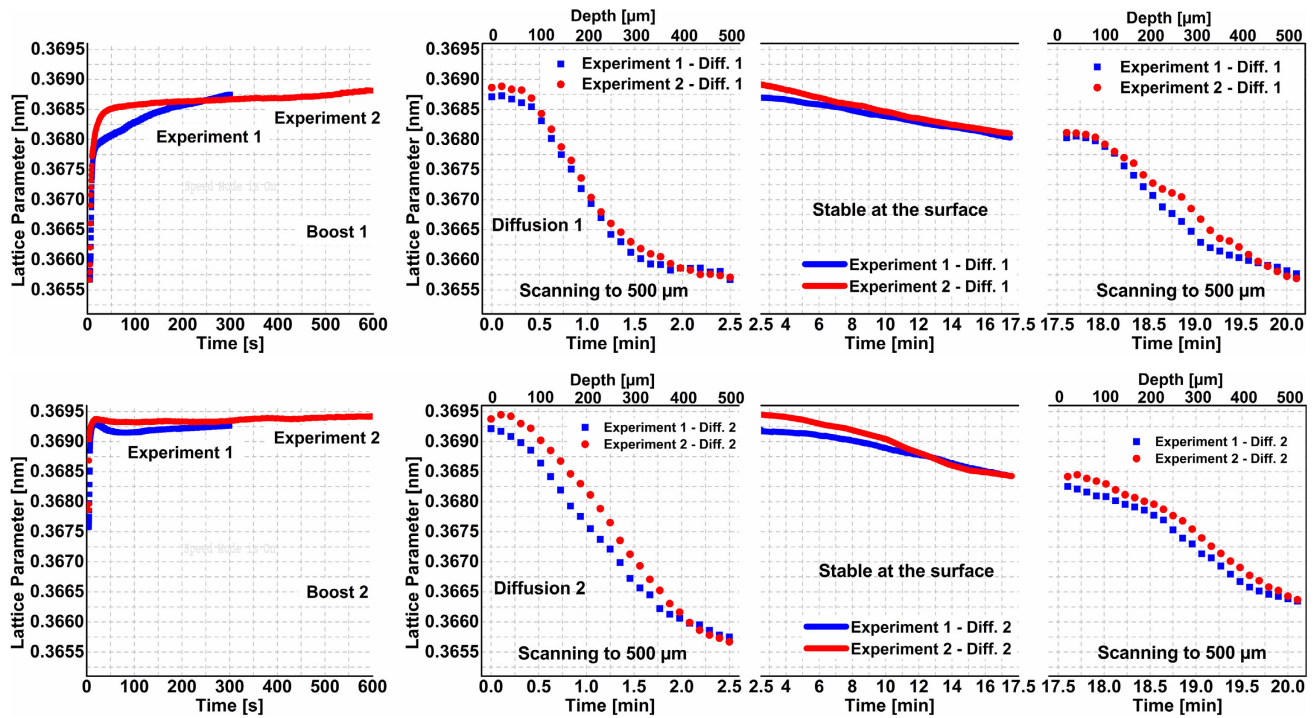
ADVANCED
SCIENCE NEWS

www.advancedsciencenews.com

ADVANCED
ENGINEERING
MATERIALS

www.aem-journal.com

Figure 12. Evolution of the lattice parameter of austenite for samples carburized with different acetylene amounts. Distances from the surface were given at the top of each figure. Figures in the middle show the carbon content evolution at the surface. The time scale starts in a place where the previous step ends. The average error bar scale is $\mp 5 \times 10^{-5}$ and it is smaller than the symbols.
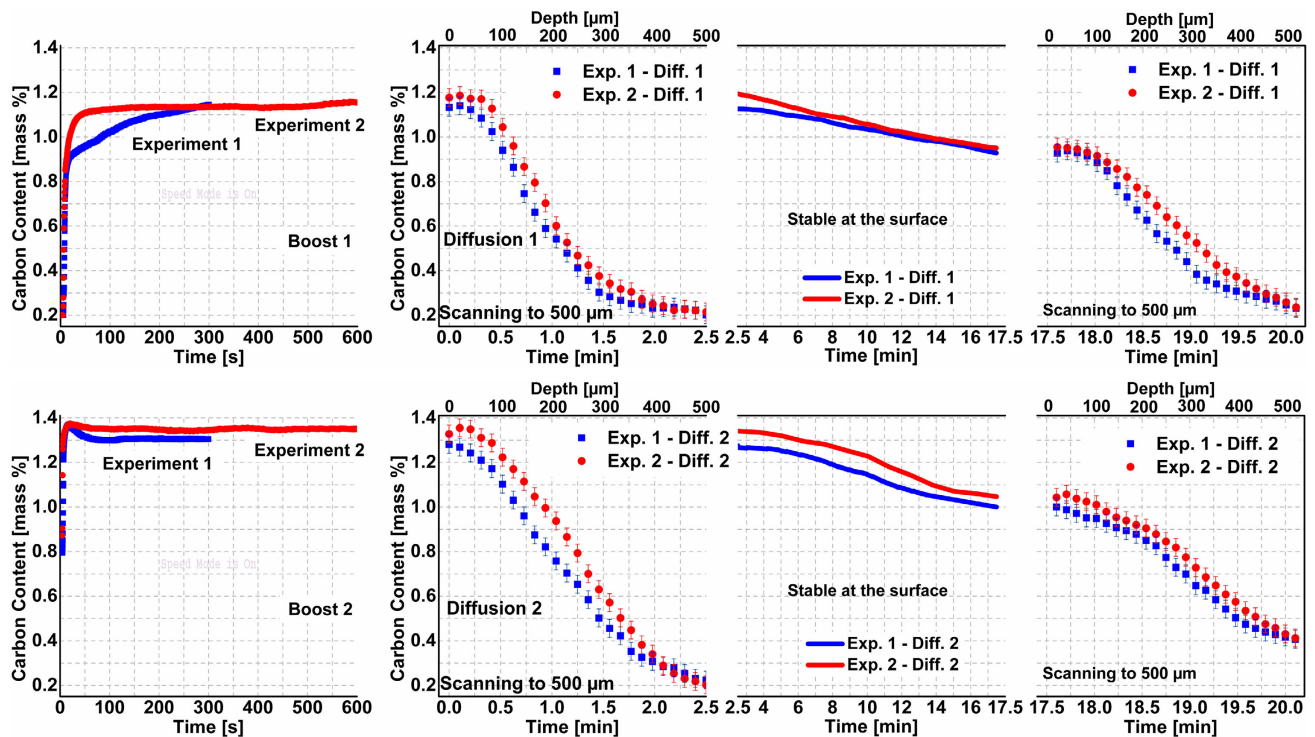
Figure 13. Change of carbon content dissolved in austenite over time during the boost and diffusion steps of two samples carburized at 940 °C with different acetylene amounts. Flow rates of experiment 1 and experiment 2 are 10 and 80 mL min^{-1}, respectively (see Table 3). The average error bar scale of ±0.04 ma% is only given for scanning stages due to the higher number of data points, but the scale is the same for all graphs.

**ADVANCED
SCIENCE NEWS**

www.advancedsciencenews.com

**ADVANCED
ENGINEERING
MATERIALS**

www.aem-journal.com
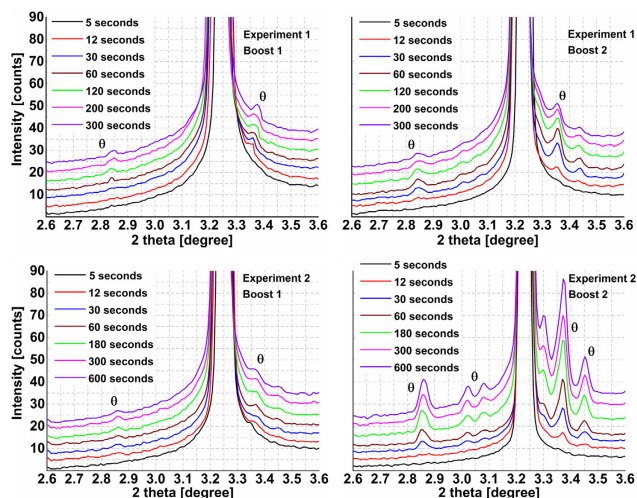
Figure 14. Diffraction patterns showing cementite (Fe₃C/θ) formation during boost steps of samples carburized with different acetylene amounts. The 5 s peak is the reference, and each peak after that was offset +3 from the previous one on the y-axis for easy examination. The temperature for all samples was 940 °C. Flow rates of experiment 1 and experiment 2 are 10 and 80 mL min^{-1} respectively (see Table 3).

For all samples, cementite started to form directly after the saturation, which lasted less than 20 s, and its amount increased until the end of the boost step. Cementite peak intensities at the second boost step of experiment 2 are apparently higher than those of the other two experiments. Therefore, we can deduce that a higher acetylene flow rate leads to increased carbide formation.

After the second boost steps, it was noted that the final carbon contents have no significant difference for experiment 1 and 2. However, if carbide formation is taken into account, which contributes to the final carbon profile by dissolution during the diffusion step, the overall effect can be seen more clearly.

Despite the difference in duration of the boost step and the acetylene flow rate, the carbon depth profiles of experiment 1 and experiment 2 are very close to each other for the first diffusion step. During the second diffusion step, the difference in the carbon profiles of these two samples increases, especially at the surface, but they are still close through the depths. This is attributed to the undissolved carbides at the surface, which did not provide extra carbon to the carbon profile in solution yet. Experiment 2 had 10 min of boost steps with a very high amount of acetylene, which led to very high carbide formation, especially for the second boost step (see Figure 14). The following 20 min of diffusion was not enough to dissolve all carbides, as shown in **Figure 15**, which shows the carbide peaks at the end of the 20 min diffusion step for all samples. The figure indicates that there are still markable cementite peaks at the surface for the sample from experiment 2, whereas the sample from experiment 1 shows very low carbides or secondary phases. It can therefore be concluded that increasing the duration of the boost step requires also a longer diffusion step for complete carbide dissolution. However,
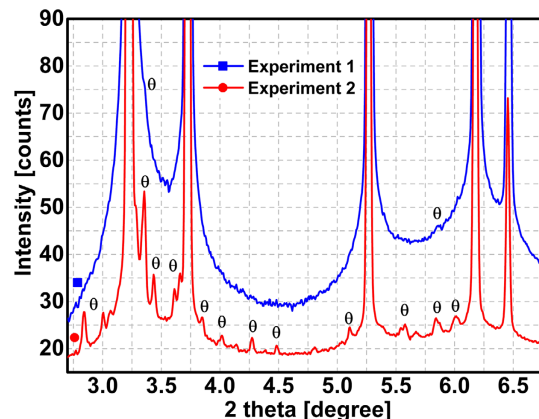
these results also clearly show that the carburizing strategy, in particular, the duration of the boost step, is a key parameter to design suitable and short carburizing processes. Very long boost steps with very high acetylene amount cause thick carbide layer formation, which slows down the acetylene diffusion from the atmosphere to the sample, and then these carbides contribute to the final carbon content by dissolution in the following steps, which is not as effective as a direct contribution.

To investigate the contribution of the carbides to the final boost step, quantitative carbide analyses were made for the final boost step of experiment 2. The higher amount of carbides made quantitative data evaluation more precise for this sample. **Figure 16** shows the determined change of cementite content during the second boost step.

Figure 15. Diffractograms showing carbide peaks near the main austenite peaks at the end of the second diffusion step measured at the surface of the samples. Cementite contents of experiment 1 and experiment 2 are 2±1 and 5±1ma%, respectively. The rest is austenite. Experiment 1 peaks were offset +10 on the y-axis for easy examination.
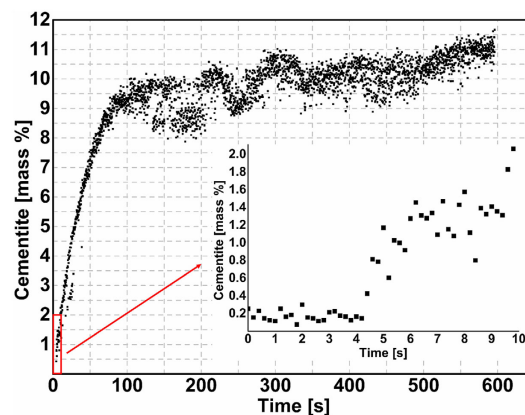

Figure 16. Change of cementite content during the second boost step of experiment 2. The small figure shows only the first 10 s in which cementite started to form. The rest of the phase fraction is austenite. Only the average error bar scale is given at the top left corner due to the higher number of data points.
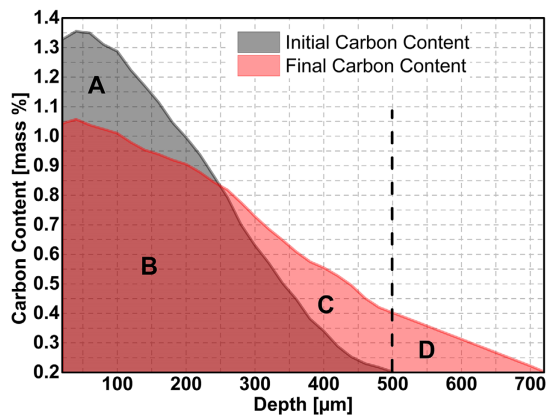
Figure 17. Initial and final carbon content distribution over depth during diffusion step 2 of experiment 2. Area A + B represents the first 2.5 min; area B + C represents the last 2.5 min of the 20 min diffusion. As scanning was done until a depth of 500 μm, area D is extrapolated to a base carbon content of 0.2 ma%.

The increase of the cementite content is similar to some examples of carbon content in austenite represented in previous sections. It starts to increase in the early stages sharply and then its increase rate slows down. The formation rate of cementite is higher in the first 100 s and then it slows down. In the small figure, which shows the carbide evolution in the first 10 s of the boost step in more detail, it can be noted that cementite formation starts after ≈5 s; i.e., it seems that the complete elimination of cementite formation is not possible. Therefore, for this case, the austenite saturation limit was reached in the first seconds and during the following 100 s of the boost step cementite formed at a very high rate. Considering that the cementite dissolves and contributes to the final carbon content, it can be concluded that a boost step duration of 100 s is not that detrimental to the process efficiency because the given acetylene is still decomposing and forms cementite. However, after 100 s of the boost step, the cementite formation rate reduces to very low levels, which means that further acetylene introduction to the furnace neither goes into solution with austenite nor forms cementite.

Figure 17 shows the initial and the final carbon content distribution of the sample from experiment 2 during the second diffusion step. By analyzing the change of area under the curve, the contribution of cementite to the final carbon content can be estimated.

This sample was chosen because cementite formation is the highest among others due to the higher acetylene flow rate. Therefore, quantitative detection of cementite is more precise. Area A + B amounts to 1.43 units and area B + C is 1.45 units. The extrapolated area D is 0.11 units. According to this estimation, ≈8.5% of the total carbon comes from the dissolution of cementite and this value has the potential to increase because it is known from the results displayed in Figure 15 that there is still ≈5 ma% of undissolved cementite at the surface of the sample after 20 min of the diffusion step. Although this an estimation, it shows that the effect of cementite could be higher for higher acetylene amounts or longer boost durations.

4.3. Effect of Boost-Diffusion Cycles

Similar to previous investigations, peak shifts were observed during the boost and diffusion steps of both experiments. These peak shifts are again directly related to carbon absorption and diffusion via the lattice parameter evolution. Integrated diffraction frames were analyzed and the lattice parameter changes were found using the same procedure as previously presented. **Figure 18** shows the change of the lattice parameter of austenite during boost and diffusion steps of two samples carburized with different parameters.

Lattice parameters are very close for both samples, especially for the first two boost-diffusion cycles. In the third boost step and following diffusion step, the lattice parameter of the CHD sample is slightly higher than that of the standard sample. Using lattice parameters and Equation (1), the change of carbon content during the boost and diffusion steps was determined and is shown in **Figure 19**.

The first two boost and diffusion steps of the two samples show a very similar tendency as the process parameters were almost identical. The final carbon contents at the end of the second boost step are very close to each other, although the standard sample has a minute longer duration of the second boost step. The possible reason for this might be the early saturation of austenite by carbon. The carbon absorption rate of the surface decreases rapidly after ≈20 s in each boost step due to austenite saturation. Further continuation of the boost steps causes carbide formation at the surface, which also contributes to the overall carbon profile by dissolution in the diffusion step, but this contribution is not as effective as direct absorption of carbon from the atmosphere. These results signify the importance of applying short but a high number of boost steps when maximum process efficiency is desired.

Although the carbon content change of the two samples is very close until the end of the second diffusion, the CHD sample has ≈0.08 ma% higher carbon than standard in the third boost-diffusion cycle. This change directly in the following cycle is unusual and not expected. This is attributed to the lower intensity gathered during boost 3 of the CHD sample as mentioned before. In Figure 7, the final intensity of the γ {111} peak is ≈45 units; however, the measurement intensity interval for all the samples is ≈55–60 units. This value was not reached for this specific example due to temperature reduction, which causes the sample to shrink. Because of this shrinkage, the beam slightly shifts to the top of the sample, where the carbon content is higher; thus, the CHD sample shows higher carbon content than the standard sample.

Similar to the previous cases, carbide formation during the boost steps was also observed in the early seconds. As carburizing parameters for the standard sample are the same as those of the CHD sample except a 1 min longer boost step, the carbide peaks look very similar. Therefore, only diffractograms of CHD samples are given in **Figure 20** to eliminate repetition.

Carbides are formed directly after saturation, which is ≈10 s. The intensity of the carbide peaks increases for each boost step. This might be because of the increase in the phase fraction of carbides or because of the intensity reduction
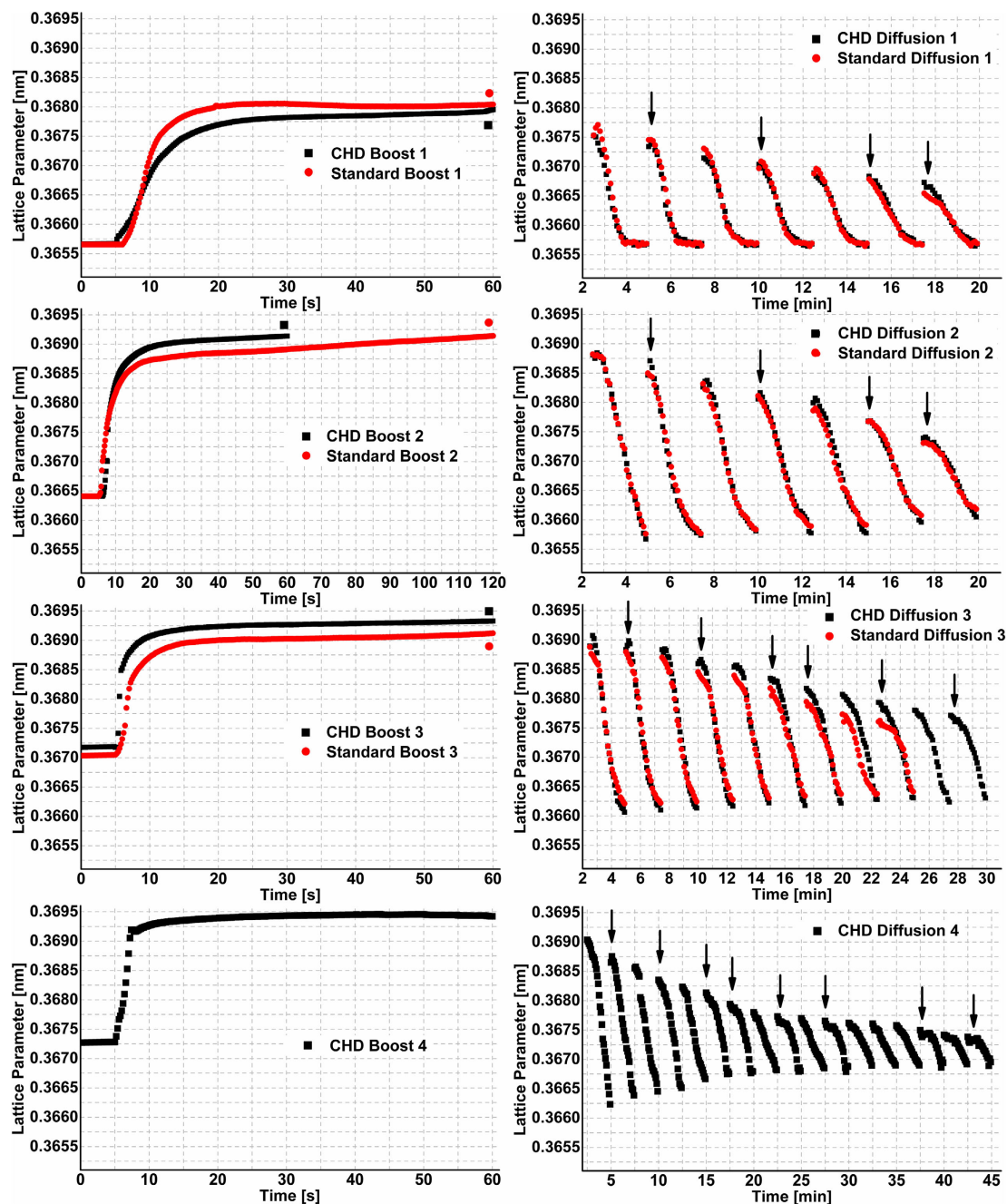
**ADVANCED
SCIENCE NEWS**
www.advancedsciencenews.com

**ADVANCED
ENGINEERING
MATERIALS**
www.aem-journal.com

Figure 18. Evolution of the lattice parameter of austenite for CHD and standard samples carburized at 940 °C. Black arrows in diffusion graphs show further investigated scans for the change of carbon content determination. The average error bar scale is $\mp 5 \times 10^{-5}$ and it is smaller than the symbols.

mentioned before. Minority phases are affected more because of this kind of slight intensity variations. Quantitative analyses of carbides were also made to boost 3 and boost 4 and represented in **Figure 21**. Cementite contents start to increase after ≈ 10 s for both samples where austenite saturation is reached according to Figure 19. For both steps, the increase rate is faster in the early stages and then reduces until the end. However, for boost 3, this difference in increase rate is not as apparent as for boost 4.

Similar to previous quantitative cementite analyses, it can be concluded that until 25 s of boost 4, acetylene supplied into the system decomposes and forms cementite. This cementite will contribute to the final carbon content by dissolution in the following diffusion step. However, after 25 s, the cementite formation rate reduces to very low levels, which means that further introduced acetylene into the system neither goes into solution with austenite nor forms cementite. Therefore, it has no contribution to the final carbon profile.
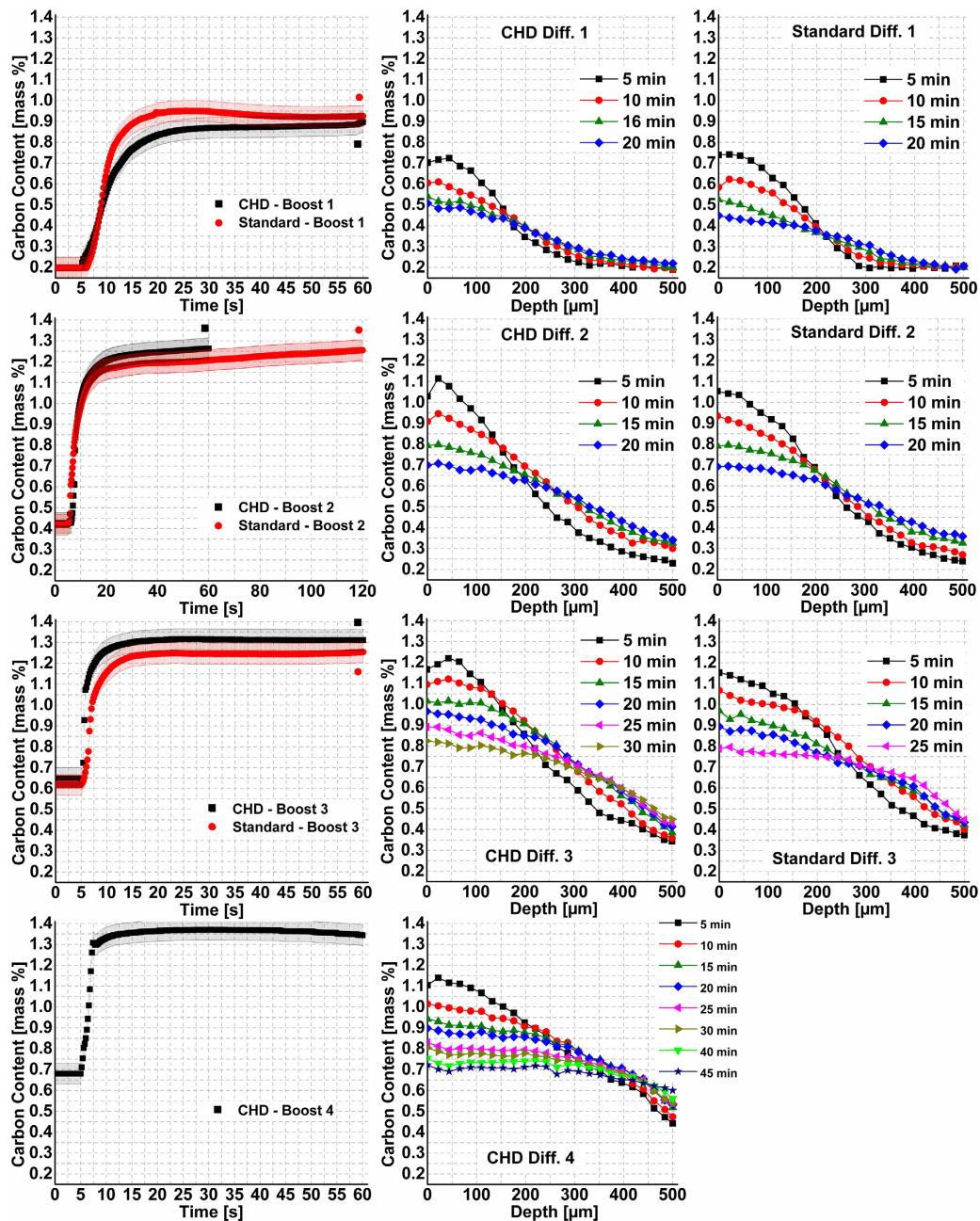
Figure 19. Carbon content change during the boost steps of the CHD sample and the standard sample carburized at 940 °C with 10 mL min^{-1} acetylene. The error bar scale is the same for diffusion steps as given in boost steps but they are not shown in the figure for the sake of clarity.

5. Conclusion

Synchrotron X-ray diffraction experiments were performed on Beamline P07-EH3 of Petra III at DESY/Hamburg during the LPC process. The main focus of this study was the boost and diffusion steps of processes conducted with different process parameters, such as temperature, duration, and amount of acetylene flow, and the number of boost steps. Collected data were analyzed using the convolution-based Rietveld refinement and experimental-based mathematical calculations to obtain information about microstructural evolution. All the findings based on those in situ diffraction data lead to the following conclusions: 1) For all samples, regardless of the process parameters, the carbon content at the surface increased rapidly at the early stages of the boost steps; i.e., the austenite saturation limit was reached quickly. Subsequently, for most of the samples, carbide peaks were observed with varying intensity after ≈20 s. After the carbide formation, the increase of carbon content in austenite reduced to very low levels or completely stopped. The main hypothesis about this phenomenon is that accumulation of
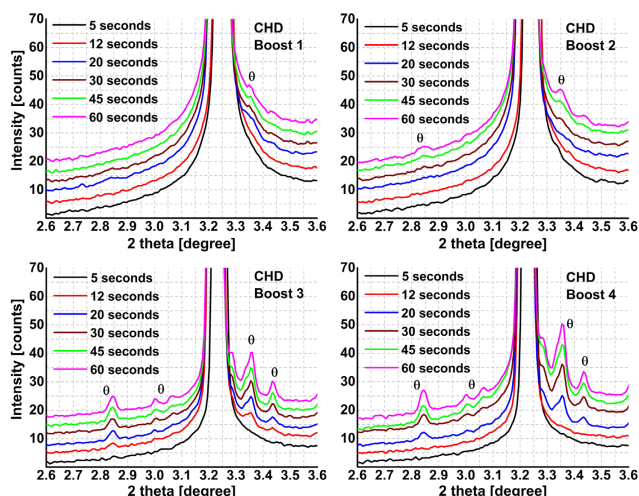
Figure 20. Diffractograms showing cementite formation during boost steps of CHD experiment. The 5 s peak is the reference; each peak after that was offset +3 from the previous one on the y-axis for easy examination.
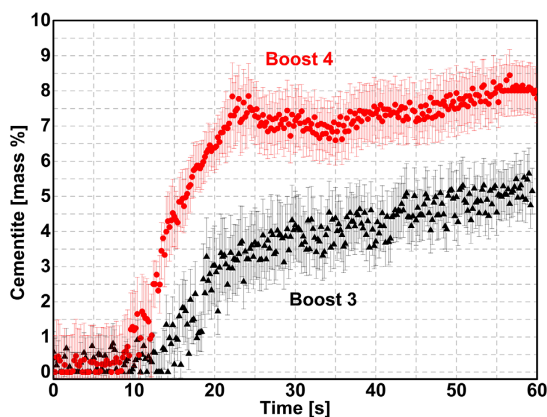

Figure 21. Change of cementite content during the third and fourth boost steps of the CHD sample.

carbon at the surface and the formed cementite layer reduced further carbon absorption from the atmosphere to the sample. Therefore, a longer duration of boost steps and higher amount of acetylene do not directly increase the carbon profile; instead, these would only increase the amount of carbides formed at the surface, and possibly at the grain boundaries, which will contribute to the carbon profile by dissolution in the following process steps. Therefore, the subsequent diffusion steps after each boost step should be adjusted accordingly. If maximum efficiency is required, a short but high number of boost steps at elevated temperature with adapted shorter diffusion steps should be applied. This conclusion correlates with a previous study.[13] 2) Higher temperature led to higher carbon absorption during the boost step. The effect of high temperature was more dominant at the early stages of the process and its effect decreased in each following step. This proves that the major driver of carbon diffusion is the carbon gradient, which flattens during the process.

Moreover, carbon reached much higher depths at a higher temperature within similar time intervals. The difference of 40 °C temperature for two processes conducted at temperatures below 1000 °C created a carbon content variation of $\approx$0.05–0.08 ma% over the carbon profile of the sample. 3) A higher acetylene flow rate led to higher carbon absorption; i.e., increasing the acetylene flow rate had a positive effect on carbon diffusion from the atmosphere to the sample. However, the rate of this effect decreases rapidly after several seconds of the boost step. This decrease is followed by a very high rate of cementite formation during the first 100 s of the boost step and furthermore, the cementite formation rate also decreases. Therefore, after that point, adding further acetylene to the system has no positive effect on the final carbon content. Moreover, for given parameters, $\approx$8.5% of the total carbon delivered to the system comes as an indirect contribution of cementite dissolution for the given case. If this contribution is also taken into consideration for the process planning, the carbon content distribution predictions can be more precise.

Acknowledgements

Conflict of Interest

The authors declare no conflict of interest.

Data Availability Statement

Research data are not shared.

Keywords

[1] J. Rudnizki, B. Zeislmair, U. Prahl, W. Bleck, *Steel Res. Int.* **2010**, *81*, 472.
[2] H. Altena, F. Schrank, *Gear Technol.* **2004**, *21*, 27.
[3] W. Gräfen, B. Edenhofer, *Surf. Coat. Technol.* **2005**, *200*, 1830.
[4] B. Edenhofer, *Heat Treat. Met.* **1999**, *26*, 1.
[5] P. Kula, R. Pietrasik, K. Dybowski, *J. Mater. Process. Technol.* **2005**, *164–165*, 876.
[6] G. Prunel, B. Stauder, *Cailiao Rechuli Xuebao/Trans. Mater. Heat Treat.* **2004**, *25*, 364.
[7] H. Altena, F. Schrank, *HTM* **2002**, *57*, 247.

[8] H. Altena, *HTM* **1994**, *49*, 58.

[9] K. Yada, O. Watanabe, *Comput. Fluids* **2013**, *79*, 65.

[10] H. Ikehata, K. Tanaka, H. Takamiya, H. Mizuno, T. Shimada, *Metall. Mater. Trans. A. Phys. Metall. Mater. Sci.* **2013**, *44*, 3484.

[11] P. Kula, K. Dybowski, E. Wolowiec, R. Pietrasik, *Vacuum* **2014**, *99*, 175.

[12] Z. Li, B. L. Ferguson, T. Yu, J. Sims, in *Therm. Process. Motion 2018 – Incl. Int. Conf. Heat Treat. Surf. Eng. Automot. Appl.*, ASM International, Geauga County, OH, USA **2018**.

[13] O. B. Tapar, J. Epp, M. Steinbacher, J. Gibmeier, *Metall. Mater. Trans. A. Phys. Metall. Mater. Sci.* **2021**, *52*, 1.

[14] L. Nobili, P. Cavallotti, M. Pesetti, *Metall. Mater. Trans. A. Phys. Metall. Mater. Sci.* **2010**, *47*, 460.

[15] H. Ikehata, K. Tanaka, H. Takamiya, H. Mizuno, *ISIJ Int.* **2012**, *52*, 1348.

[16] M. Steinbacher, B. Clausen, T. Lübben, H. Surm, *HTM – J. Heat Treat. Mater.* **2012**, *67*, 65.

[17] G. Ashiotis, A. Deschildre, Z. Nawaz, J. P. Wright, D. Karkoulis, F. E. Picca, J. Kieffer, *J. Appl. Crystallogr.* **2015**, *48*, 510.

[18] A. A. Coelho, *J. Appl. Crystallogr.* **2018**, *51*, 210.

[19] J. Epp, J. Dong, H. Meyer, A. Bohlen, *Scr. Mater.* **2020**, *177*, 27.

[20] B. Gornicki, *Gear Solut.* **2015**.

[21] T. Mendiara, M. P. Domene, A. Millera, R. Bilbao, M. U. Alzueta, *J. Anal. Appl. Pyrolysis* **2005**, *74*, 486.

[22] H. W. Antes, *Heat Treat. Prog.* **2005**, *8*, 51.

[23] E. Wołowiec-Korecka, M. Korecki, M. Sut, A. Brewka, P. Kula, *Metals* **2019**, *9*, 439.

[24] M. Steinbacher, *Thermogravimetrische Messungen Beim Niederdruckaufkohlen Als Grundlage Für Simulationen*, Bremen University, Bremen, Germany **2012**.

[25] M. Onink, C. M. Brakman, F. D. Tichelaar, E. J. Mittemeijer, S. van der Zwaag, J. H. Root, N. B. Konyer, *Scr. Metall. Mater.* **1993**, *29*, 1011.

[26] R. U. Khan, D. Buchholz, F. Graf, R. Reimert, *Int. J. Chem. React. Eng.* **2009**, *7*, A10.

[27] M. Sugiyama, K. Ishikawa, H. Iwata, *Adv. Mater. Process.* **1999**, *155*, 29.

[28] B. Esper, *Ind. Heat.* **2009**.

[29] M. Steinbacher, B. Clausen, F. Hoffmann, H. W. Zoch, *HTM – J. Heat Treat. Mater.* **2008**, *63*, 33.

[30] A. Schneider, G. Inden, *Calphad Comput. Coupling Phase Diagrams Thermochem.* **2007**, *31*, 141.

[31] B. Ozturk, V. L. Fearing, J. A. Ruth, G. Simkovich, *Solid State Ionics* **1984**, *12*, 145.

[32] R. J. Madix, *Adv. Catal.* **1980**, *29*, 1.

[33] R. Neubauer, C. M. Whelan, R. Denecke, H. P. Steinrück, *J. Chem. Phys.* **2003**, *119*, 1710.

[34] R. Byron Bird Warren, E. Stewart Edwin, N. Lightfoot, R. B. Bird, W. E. Stewart, E. N. Lightfoot, *Transport Phenomena*, 2nd ed., John Wiley & Sons, Inc, New York, USA **2006**.